

Interacting electrons in the Aharonov-Bohm interferometer

S. Ihnatsenka and I. V. Zozoulenko

*Solid State Electronics, Department of Science and Technology,
Linköping University, 60174 Norrköping, Sweden*

(Dated: November 8, 2018)

We present a microscopic picture of quantum transport in the Aharonov-Bohm (AB) interferometer taking into account electron interaction within the Hartree and the spin density functional theory approximations. We discuss the structure of the edge states for different number of the Landau levels in the leads, their coupling to the states in the central island and the formation of compressible/incompressible strips in the interferometer. Based on our results we discuss the existing theories of the unexpected AB periodicity, which essentially rely on specific phenomenological models of the states and their coupling in the interferometer. Our work provides a basis for such the theories, giving a detailed microscopic description of the propagating states and the global electrostatics in the system at hand.

PACS numbers: 73.23.Ad, 73.21.La, 73.23.Hk, 72.15.Gd

I. INTRODUCTION

The recent years have witnessed a renewed interest in studies of magnetotransport in quantum Hall systems in confined geometries^{1,2,3,4,5,6,7}. These studies are motivated in part by the prospect of topological quantum computing^{5,6,7} as well as by fundamental interest to explore novel exciting physics related to e.g. exotic fractional statistics in two dimensional systems¹. Some recent studies have revealed new unexpected features in systems that have been extensively studied in the nighties and that seemed to be well understood since long time ago. This includes, for example, an unexpected periodicity of the Aharonov-Bohm (AB) electron interferometer in the integer quantum Hall regime of the edge state transport revealed in the experiments of Camino *et al.*^{2,3}

A typical Aharonov-Bohm interferometer^{2,3,8,9,10,11} includes an electron island coupled to the leads by two quantum point contacts (QPCs), see Fig. 1 (a). At a given magnetic field there are f_{leads} propagating edge states in the leads. The electron density in the constrictions of the QPC is smaller than in the leads, and hence only the lowest f_c states are fully transmitted through the constriction, whereas the remaining highest $f_{leads} - f_c$ states are partially or fully reflected. A typical conductance of the AB interferometer as a function of magnetic field exhibits a step-like structure with plateaus separated by wide transitions regions^{2,3,8,9,10,11}. This structure of the conductance reflects successive depopulation of the magnetosubbands in the constrictions. The plateau regions correspond to the field regions where the QPC openings are fully transparent (the transmission coefficient through an individual QPC is integer, $T \cong f_c$), and transition regions between these plateaus correspond to the partial transparent QPC openings (the transmission coefficient is non-integer, $f_c < T < f_c + 1$). In the latter case, reflection on the QPC openings inside the island confines the partially transmitted $(f_c + 1)$ -th state between two QPCs which gives rise to pronounced AB conductance oscillations in the transition regions between

the plateaus. Note that in the weak coupling regime when the number of propagating states in the constrictions is reduced below one, $f_c = 0$, the AB oscillations are suppressed by the single electron charging effects.^{9,10,11} In this case the charge of the electron island inside interferometer becomes quantized, and the conductance exhibits familiar Coulomb blockade (CB) peaks corresponding to addition/removing one electron to/from the interior of the central island.

According to the conventional theory of the Aharonov-Bohm interferometer its conductance shows a peak each time the enclosed flux $\phi = BS$ changes by the flux quantum $\phi_0 = h/e$, $\Delta(BS) = \phi_0$.¹² Thus, the conductance of the interferometer as a function of the magnetic field exhibits the periodicity

$$\Delta B = \frac{\phi_0}{S}, \quad (1)$$

with S being the area of the island. The inclosed flux through the interferometer can also be varied at a fixed magnetic field by changing a gate voltage. In the case when the area changes linearly with the change in the gate voltage, $\Delta S = \alpha \Delta V_g$, the expected periodicity is

$$\Delta V_g = \phi_0 / \alpha B. \quad (2)$$

The first experimental study of the AB interferometer in lateral GaAs heterostructures was performed by van Wees *at al.*⁸ They reported a good agreement between the theory and experiment with some deviation from Eq. (1) for the case of several propagating modes in the constrictions ($f_c \geq 2$). They attributed this deviation to the effect of magnetic field on the location of the edge states corresponding to different f_c . Since these pioneering experiments, the interpretation of the AB oscillations based on Eq. (1) has been widely accepted. However, in recent experiments of Camino *et al.*^{2,3} the validity of the conventional theory of the AB oscillations in lateral semiconductor heterostructures has been questioned. In particular, Camino *et al.* demonstrated that periodicity of the AB oscillations as a function of the magnetic field

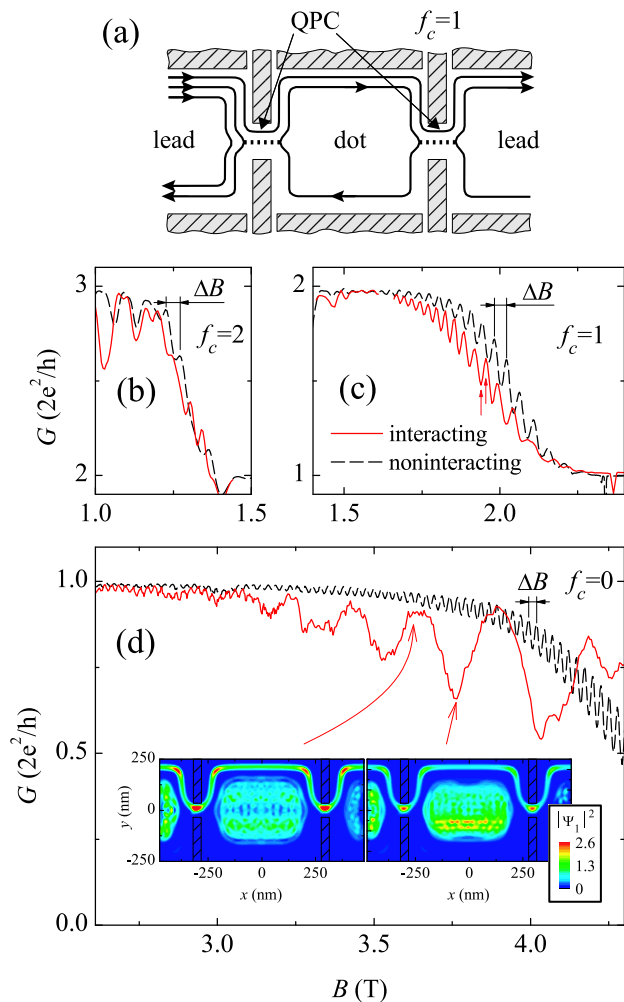


FIG. 1: (color online) (a) Schematic geometry of the AB interferometer. Shaded regions corresponds to the metallic gates on the top of the GaAs heterostructure. The geometrical size of the dot is $500 \times 520 \text{ nm}^2$. The diagram illustrates the case of $f_c = 1$ and $f_{lead} = 3$ corresponding to one fully transmitting states through the constrictions and 3 propagating states in the leads (for the calculated wave function for this case see Fig. 4). (b), (c), (d) The AB oscillations for respectively $f_c = 2, 1, 0$ calculated for interacting and noninteracting electrons (solid and dashed lines respectively). ΔB shows the expected periodicity according to Eq. (1). The arrows in (c) indicate the magnetic fields corresponding to calculated LDOS shown in Fig. 3. The inset in (d) illustrates the wave function due to the first propagating state in the leads.

depends of the number of fully transmitted states in the constriction f_c and is well described by the dependence

$$\Delta B = \frac{1}{f_c} \frac{\phi_0}{S}, \quad (3)$$

which obviously differs by a factor $1/f_c$ from the conventional formula (1). On the other hand, the back-gate charge period is the same (one electron) for all f_c , independent of on the magnetic field in stark contrast to Eq. (2). Moreover, Camino *et al.*² re-analyzed the data of

the experiment of van Wees *et al.*⁸ and concluded that it is, within the experimental uncertainty, also described by Eq. (3). (Note that the same re-interpretation of the van Wees *et al.* experiment was first proposed by Dharma-wardana *et al.*¹³)

It should be stressed that Eqs. (2)-(3) represent a significant departure from the conventional description of the AB oscillations based on Eq. (1). The latter relies on a one-electron picture of non-interacting electrons, whereas the former require accounting for electron interaction and/or CB charging effects. An interplay between the AB and CB oscillations has been experimentally studied by Taylor *et al.*¹⁰ and Field *et al.*¹¹ Taylor *et al.*¹⁰ has established a simple condition for the onset of the CB oscillations in their structure, namely the dot has to be in the weak coupling regime with only partially transmitted states in the constrictions, $f_c = 0$. On the contrary, Field *et al.*¹¹ found coexistence of the AB and CB oscillations extended even into the open dot regime when $f_c \geq 2$. A persistence of the Coulomb blockade oscillations into the open regime $f_c \geq 1$ was also discussed by Alphenaar *et al.*⁹. Note that possibility of the Coulomb charging effects in the strongly coupled regime has been a subject of interesting discussions for the case of quantum antidots in the integer quantum Hall regime¹⁴ as well as open quantum dots at zero magnetic field¹⁵. It should be also mentioned that similar deviations from the standard AB formula that are also well described by Eq. (3) have been very recently reported by Goldman *et al.*¹⁶ for the case of an *antidot-based* AB interferometer.

The effect of electron interaction and Coulomb charging on the conductance of the AB interferometer in the open regime of $f_c \geq 1$ was studied by Dharma-wardana *et al.*¹³ and very recently by Rosenow and Halperin⁴. Using different approaches they both arrived to the same conclusion that the AB oscillations can be modulated by CB-type effect leading to the novel periodicity of the oscillations described by Eq. (3). However, their models have been based on very different microscopic mechanisms of interaction and charging in the interferometer. In the model of Dharma-wardana *et al.*¹³ the predicted modulation is due to the enhanced screening of the usual CB oscillations by fully transmitted states through constriction effectively acting as metallic strips. In contrast, the predictions of Rosenow and Halperin⁴ are based on the assumption of the coupling between the states in the leads and the central compressible island inside the interferometer.

Thus, understanding of the role of electron interaction and charging in the AB interferometer and identification of the origin of the unexpected periodicity of the oscillations (3) require detailed knowledge of the microscopic structure as well as the coupling strength between different states in the leads and in the central island. To the best of our knowledge such calculations have not been reported in the literature yet. At the same time, this information is essential in theories like those developed in

Refs. [4,13] that rely on specific models of the coupling between states in the interferometer.

In the present paper we perform such the calculations for the AB interferometer in the integer quantum Hall regime where electron interaction and spin effects are included within the spin-density functional theory (DFT). The utilized approach corresponds to the first-principles magnetoconductance calculations (within the effective mass approximation) that start from a geometrical layout of the device, are free from phenomenological parameters of the theory, and do not rely on model Hamiltonians.^{17,18} The power of this approach has been recently demonstrated for related systems (quantum dots and quantum wires) where a *quantitative* agreement with the corresponding experiments has been achieved^{19,20}.

The paper is organized as follows. A brief description of the model is given in Sec II. Section III presents results for the edge state structure and coupling between states in the leads and in the dot calculated within the Hartree approximation as well as within the spin-DFT approach. We discuss the obtained results and outline their relation to the experiment and existing theories in Sec. IV. The conclusion is presented in Sec. V.

II. MODEL.

We consider an electron interferometer defined by split-gates in the GaAs heterostructure in an open quantum dot geometry similar to those studied experimentally^{2,3,8,9,10,11}, see Fig. 1. The geometrical size of the dot is $500 \times 520 \text{ nm}^2$, the geometrical width of the QPC openings is 80 nm, and the distance from the two-dimensional electron gas to the surface is $b = 50 \text{ nm}$. The Hamiltonian of the whole system (the island + the semi-infinite leads) in the framework of the density-functional theory (DFT) within the Kohn-Sham formalism²¹ can be written in the form $H = H_0 + V(\mathbf{r})$, where

$$H_0 = -\frac{\hbar^2}{2m^*} \left\{ \left(\frac{\partial}{\partial x} - \frac{eiBy}{\hbar} \right)^2 + \frac{\partial^2}{\partial y^2} \right\} \quad (4)$$

is the kinetic energy in the Landau gauge, and the total confining potential

$$V(\mathbf{r}) = V_{conf}(\mathbf{r}) + V_H(\mathbf{r}) + V_{xc}^\sigma(\mathbf{r}) + V_Z, \quad (5)$$

where $V_{conf}(\mathbf{r})$ is the electrostatic confinement (including contributions from the top gates, the donor layer and the Schottky barrier), $V_H(\mathbf{r})$ is the Hartree potential,

$$V_H(\mathbf{r}) = \frac{e^2}{4\pi\epsilon_0\epsilon_r} \int d\mathbf{r}' n(\mathbf{r}') \left(\frac{1}{|\mathbf{r} - \mathbf{r}'|} - \frac{1}{\sqrt{|\mathbf{r} - \mathbf{r}'|^2 + 4b^2}} \right), \quad (6)$$

where $n(\mathbf{r})$ is the electron density, the second term corresponds to the mirror charges situated at the distance b from the surface, $\epsilon_r = 12.9$ is the dielectric constant of

GaAs. $V_{xc}^\sigma(\mathbf{r})$ is the exchange-correlation potential in the local spin-density approximation where σ stands for spin-up, \uparrow , and spin-down, \downarrow , electrons, and V_Z is a standard Zeeman term. In calculation of $V_{xc}^\sigma(\mathbf{r})$ we utilized a commonly used parametrization of Tanatar and Ceperly²². (A detailed description of the Hamiltonian can be found in Refs. 17,18). The dot and the leads are treated on the same footing, i.e. the electron interaction and the magnetic field are included both in the lead and in the dot regions. In what follows we will mostly concentrate on the Hartree approximation (i.e. when $V_{xc}^\sigma(\mathbf{r}) = 0$). This is because the main conclusions concerning the Aharonov-Bohm oscillations in the system at hand are qualitatively similar for the spinless Hartree case ($V_{xc}^\sigma(\mathbf{r}) = 0$) and the spin-resolved DFT case ($V_{xc}^\sigma(\mathbf{r}) \neq 0$).

We calculate the self-consistent electron densities, potentials and the conductance on the basis of the Green's function technique. The description of the method can be found in Refs. 17,18 and thus the main steps in the calculations are only briefly sketched here. First we compute the self-consistent solution for the electron density, effective potential and the Bloch states in the semi-infinite leads by the technique described in Ref. 23. Knowledge of the Bloch states allows us to find the surface Greens function of the semi-infinite leads. We then calculate the Green's function of the central section of the structure by adding slice by slice and making use of the Dyson equation on each iteration step. Finally we apply the Dyson equation in order to couple the left and right leads with the central section and thus compute the full Green's function $\mathcal{G}^\sigma(E)$ of the whole system. The electron density is integrated from the Green's function (in the real space),

$$n^\sigma = -\frac{1}{\pi} \int_{-\infty}^{\infty} \Im[\mathcal{G}^\sigma(\mathbf{r}, \mathbf{r}, E)] f_{FD}(E - E_F) dE, \quad (7)$$

where f_{FD} is the Fermi-Dirac distribution. This procedure is repeated many times until the self-consistent solution is reached; we use a convergence criterium $|n_i^{out} - n_i^{in}| / (n_i^{out} + n_i^{in}) < 10^{-5}$, where n_i^{in} and n_i^{out} are input and output densities on each iteration step i .

Finally the conductance is computed from the Landauer formula, which in the linear response regime is

$$G^\sigma = -\frac{e^2}{h} \int_{-\infty}^{\infty} dE T^\sigma(E) \frac{\partial f_{FD}(E - E_F)}{\partial E}, \quad (8)$$

where the transmission coefficient for the spin channel σ , $T^\sigma(E)$, is calculated from the Green's function between the leads.^{17,18} All the calculations reported in the present paper are performed for the temperature $T = 0.2\text{K}$.

To outline the role of the electron interaction we also calculate the conductance of the open dot in the Thomas-Fermi (TF) approximation where the self-consistent electron density and potential are given by the standard TF equation at zero field. This approximation does not capture effects related to electron-electron interaction in quantizing magnetic field such as formation of compressible and incompressible strips and hence it corresponds

to noninteracting one-electron approach where, however, the total confinement is given by a smooth fixed realistic potential, see Refs. 17,18 for details.

In order to provide correct interpretation of the results reported in this paper, it is important to outline the validity and limitations of the present approach. Our calculations correspond to a so-called “standard approach”²⁴ based on the ground-state DFT in the Landauer formula. It has been demonstrated that this approach accurately describes the conductance in the regime of the strong coupling when the conductance of the QPCs connecting the device region and the leads exceeds the conductance unit $G_0 (= 2e^2/h$ for the spin-degenerate electrons). This corresponds to the case when charge quantization inside the device is not expected to occur. In this regime the “standard approach” was shown to reproduce not only qualitatively, but in many cases even quantitatively the observed conductance of metallic nanowires²⁴ as well as GaAs lateral heterostructures^{19,20}.

However, the reliability of this approach has been questioned for the case of the weak coupling where the QPC conductance drops below the conductance unit G_0 such that charge inside the device becomes quantized (i.e. in the Coulomb blockade regime)^{18,24,25}. This is due to the uncorrected self-interaction errors in the standard DFT approach (related to the lack of the derivative discontinuity in the exchange-correlation potential) for the case when localization of charge is expected to occur. Because of this, we do not expect the present approach to provide a reliable conductance for the case of the weak coupling $f_c = 0$ (Fig. 1 (d)), where the experiments exhibit the Coulomb blocked conductance^{9,10}.

While the present approach is not expected to account for single-electron tunneling in the conductance (leading to the Coulomb blockade peaks), one can expect that it correctly reproduces a global electrostatics of the interferometer and microscopic structure of the quantum mechanical edge states regardless whether the conductance is dominated by a single-electron charging or not. This is because the interferometer contains a large number of electrons, $\sim 400 - 500$, and thus the electrostatic charging caused by a single electron hardly affects the total confining potential of the interferometer. Thus the results of the present study provide an accurate information concerning the locations of the propagating states and the structure of compressible/incompressible strips in the interferometer. Our calculations are also expected to provide a detailed information concerning the coupling strengths between the states in the leads and in the island.

III. RESULTS

Figure 1 (b)-(d) shows the conductance of the AB interferometer as a function of magnetic field for spin-degenerate interacting (Hartree) and noninteracting (Thomas-Fermi) electrons for different numbers of fully

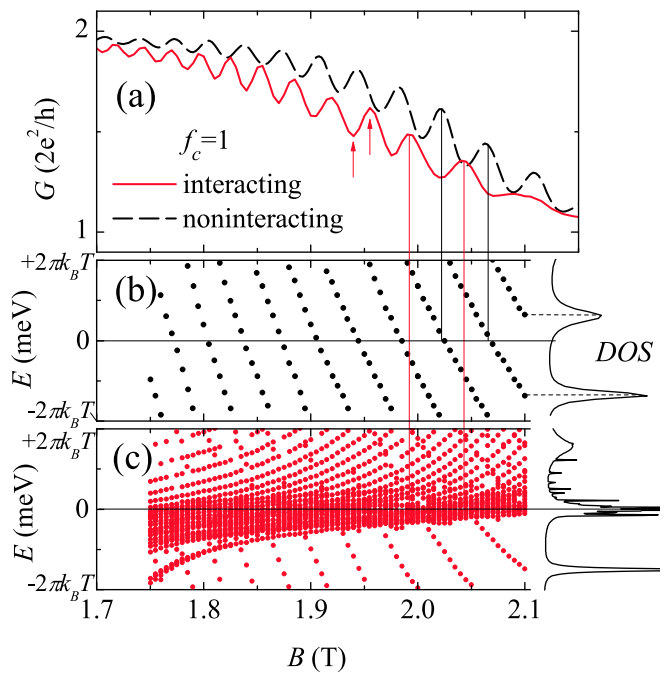


FIG. 2: (color online) (a) The magnetoconductance of the AB interferometer for $f_c = 1$ for interacting and noninteracting spinless electrons (The arrows in (a) indicate the magnetic fields corresponding to calculated LDOS shown in Fig. 3). Evolution of the resonant energy levels in the vicinity of E_F for (b) noninteracting and (c) interacting electrons. The insets show DOS in the dot for the specified value of the field $B = 2.1$ T; note that evolution of the energy levels was obtained from the peak positions of the DOS at each given value of B .

propagating channels f_c in the QPC openings, $f_c = 2, 1, 0$. In these figures the voltages on the gates defining the QPCs are set such that the constrictions accommodate f_c fully transmitted (lowest) Landau levels, while the $(f_c + 1)$ -th Landau level is only partially transmitted.

Let us first concentrate on the cases $f_c = 1$ and $f_c = 2$ when the conductance shows the Aharonov-Bohm oscillations with the same periodicity of $\Delta B = 0.025$ T. This periodicity is in excellent agreement with the conventional AB formula (1) where the actual dot area $S \approx 410 \times 410$ nm² is slightly smaller than the geometric dot area $S_{act} = 500 \times 520$ nm². The Aharonov-Bohm oscillations can be related to evolution of the corresponding dot spectrum when a single-electron states cross the Fermi level each time the flux through the dot increases by the flux quantum. For the case of noninteracting electrons this is illustrated in Fig. 2 (b) which shows an evolution of the resonant levels as a function of magnetic field in the vicinity of the Fermi energy. [To obtain the evolution of the resonant levels we analyze the density of states (DOS) in the dot at each given B and plot the positions of the peaks in the DOS as B varies as illustrated in Fig. 2 (b); see also illustration of the DOS and the local density of states (LDOS) shown in Fig. 3]. Figure 2 (b) shows that

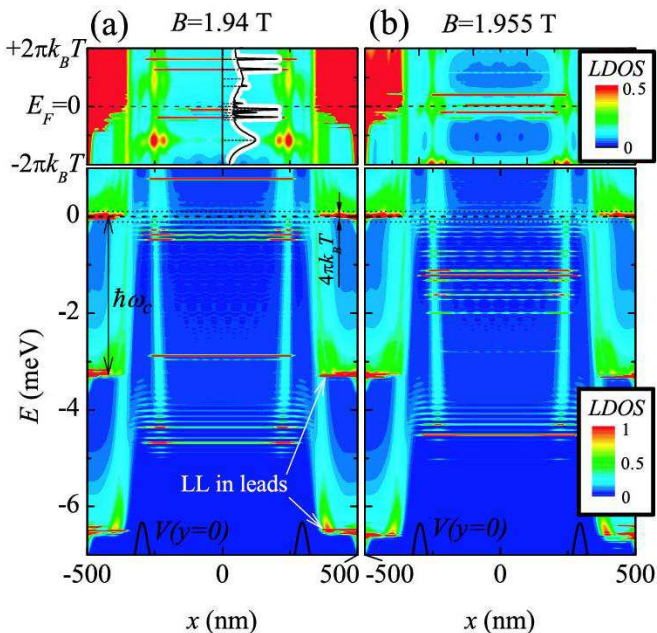


FIG. 3: (color online) The local density of states (LDOS) in the interferometer for the case $f_c = 1$ (spinless interacting electrons, Hartree approximation). (a) and (b) correspond to a consecutive maximum and minimum of the AB oscillations indicated by arrows in Fig. 2(a). The upper panels show resonant levels in the vicinity of E_F in an enlarged scale illustrating the resonant tunneling mediated by the broad resonant levels of the quantum dot as well as showing the effect of pinning of narrow resonances to E_F .

the dot conductance exhibits a maximum each time a resonant state sweeps past E_F . The resonant levels giving rise to the AB oscillations are rather broad (with broadening $\Gamma \sim kT$) because they are situated close to the dot boundaries and their coupling to the states in the leads is rather strong.

Figure 2 (c) shows an evolution of the resonant levels for the case of interacting electrons. As for the case of noninteracting electrons, the AB oscillations can be traced to relatively broad resonant levels that sweep past the Fermi level each time the flux through the dot increases by the flux quantum. However the resonant level structure of the interacting electrons exhibits qualitatively new features. In addition to the broad levels mediating the AB oscillations, the DOS shows many narrow resonances concentrating near E_F . These resonances correspond to the states residing inside the dot that are very weakly coupled to the leads (hence small broadening). These states clearly show pinning to the Fermi level (see Refs. 17,20 for a detailed discussion of the pinning effect in open quantum dots). However, the pinning of the inner states to the Fermi energy does not imply that a compressible island forms in the middle of the interferometer. Indeed, Fig. 3 shows the local density of states (LDOS) integrated in the transverse (y -direction). In the magnetic field interval under consideration (correspond-

ing to $f_c = 1$) there are three propagating states in the leads with the highest one being always pinned to E_F (see also Fig. 4 (c) depicting the magnetosubband structure in the leads). The dot itself shows the Darwin-Fock type energy spectrum with a clear signature of the Landau level (LL) condensation when the resonant levels concentrate around LLs of the corresponding two-dimensional electron gas. Clearly, the upper bunch of levels (concentrating around the second LL) is not pinned to the E_F . The pinning of the highest LL to the E_F (as well as the accompanying formation of the compressible strip inside the dot) occurs at much higher fields far above interval $f_c = 1$. Thus the pinning of several resonant levels to E_F for the case $f_c = 1$ shown in Figs. 2 (c), 3 represents an onset of formation of the compressible island in the middle of the interferometer. It can be mentioned that a related question whether the compressible strips form in an *antidot-based* AB interferometer, has been a subject of recent debate²⁶.

Despite of the difference in the structure of the DOS for interacting and noninteracting electrons, their conductance is practically the same (the small shift of the conductance curves relative to each other is due to a small difference between the Hartree and TF densities). To understand the reason for this, we inspect the wave functions in the interferometer, see Fig. 4. We focus on the case of $f_c = 1$ when the first state in the leads $N_{lead} = 1$ passes almost adiabatically through the QPC, the third state $N_{lead} = 3$ is reflected, and the AB oscillations are mostly due to the second state $N_{lead} = 2$ which is partially transmitted through the QPC (see Fig. 5 illustrating the transmission coefficients for $f_c = 1$ and $f_c = 2$). In the field interval under consideration a compressible strip in the leads forms only for the highest state $N_{lead} = 3$ (a corresponding band structure for the lead is shown in Fig. 4). Two lowest states, $N_{lead} = 1, 2$, are not compressible and thus their respective spatial location and structure are very similar for interacting and noninteracting electrons. As a result, the coupling of these states to the states in the dot are almost the same for interacting and noninteracting electrons, and therefore the corresponding conductances are practically the same. It should also be mentioned that in accordance to the discussion above the wave function pattern does not show an evidence of the formation of the compressible island in the center of the interferometer. In contrast, the compressible strip corresponding to $N_{lead} = 3$ is clearly seen in the leads.

For higher magnetic fields when a number of transmitted channels in the QPC is reduced below one, $f_c = 0$, the electron interaction becomes strongly pronounced leading to smearing out the AB oscillations and to emergence of a new oscillation pattern, Fig. 1 (d). For higher magnetic field the compressible strip forms in the center of the dot. As a result, the electrons are scattered directly in and out of this region instead of following well defined closed paths along the dot perimeter, see the inset to Fig. 1 (d). This leads to the suppression of the AB oscillations and emergence of a new pattern which periodicity

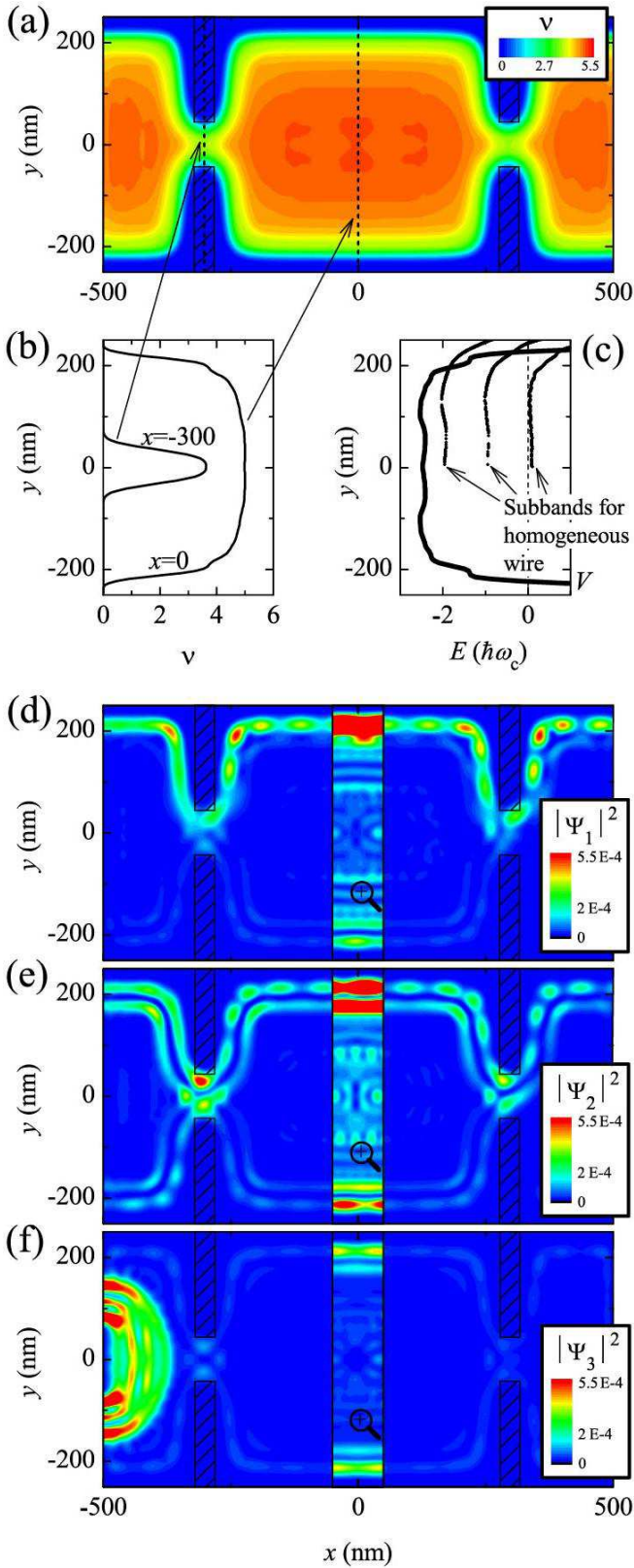


FIG. 4: (color online) (a),(b) The local filling factor $\nu(x, y)$ calculated for spinless interacting electrons (Hartree approximation) for $f_c = 1$. (c) the total confining potential (thick line) and the corresponding subband structure of an infinite quantum wire. (d)-(f) the wave functions modulus at $B = 1.955$ T corresponding respectively to the first, second and the third propagating states in the leads. The third subband being pinned at the Fermi energy $E_F = 0$ forms a compressible strip in the center of the wire. The insets in (d)-(f) show strongly 10 times magnified intensity of the wave functions in the middle section of the interferometer.

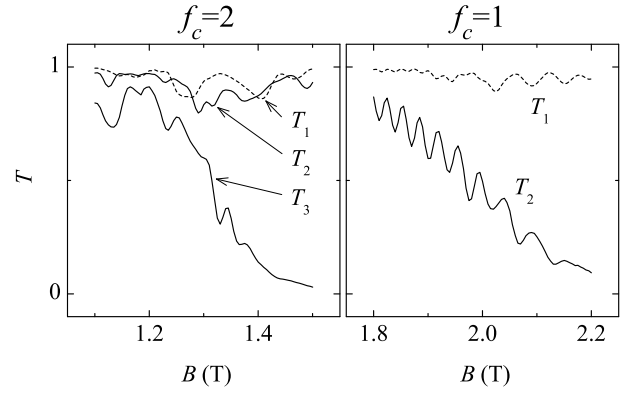


FIG. 5: Transmission coefficients $T_i = \sum_j T_{ji}$ from i -th mode in the left lead to all available j -th modes in the right leads for interacting spinless electrons (Hartree approximation) for (a) $f_c = 2$ and (b) $f_c = 1$. (Note that corresponding total transmission is shown in Fig.1 (b), (c).)

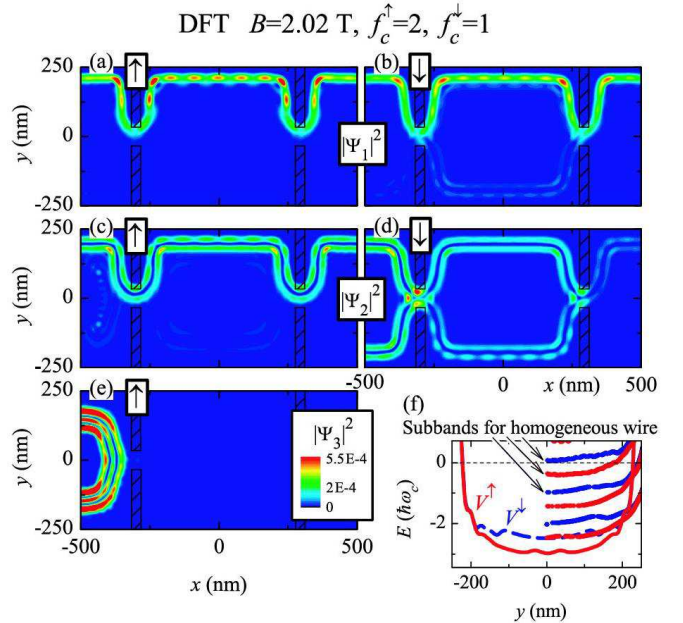


FIG. 6: (color online) The wave functions modulus at $B = 2.025$ T calculated within the spin-DFT approximation $f_c = f_c^\uparrow + f_c^\downarrow = 3$ ($f_c^\uparrow = 2, f_c^\downarrow = 1$). Left and right columns correspond to the spin-up and spin-down electrons. For a given magnetic fields there are five propagating states in the leads (as illustrated in the band diagram showed in (f)), three spin-up states and two spin-down states. Panels (a)-(e) show the wave functions corresponding to these states.

$\Delta B \approx 0.22$ T is consistent with the area of a compressible strip inside the dot ($\sim 135 \times 135$ nm²). It should be mentioned that the non-interacting approach (where no compressible strips are present) always shows a perfect AB periodicity.

We also calculated the spin-resolved conductance $G^\sigma = G^\sigma(B)$ within the DFT approach with the exchange-correlation effects included in the local spin density ap-

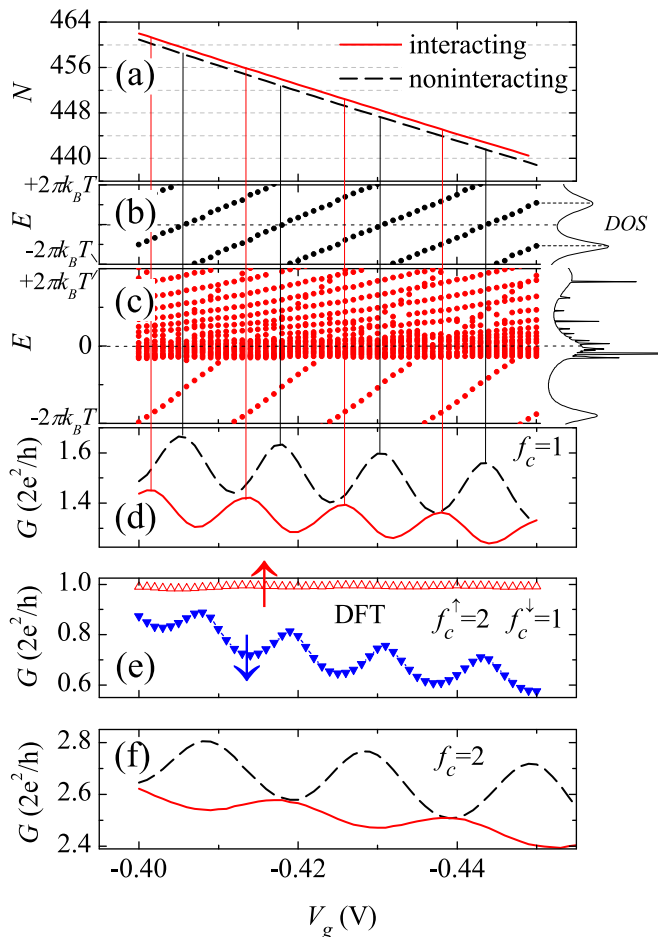


FIG. 7: (color online) (a) The number of electrons inside the dot of the AB interferometer for $f_c = 1$ for interacting and noninteracting spinless electrons as a function of the gate voltage V_g . Evolution of the resonant energy levels in the vicinity of E_F for (b) noninteracting and (c) interacting electrons. The insets in (b), (c) show DOS in the dot for the specified value of the field $V_g = -0.45$ V; note that evolution of the energy levels was obtained from the peak positions of the DOS at each given value of V_g . Conductance of interacting and noninteracting spinless electrons for (d) $f_c = 1$ and (f) $f_c = 2$. (e) Spin-DFT conductance of the AB interferometer for $f_c = f_c^\uparrow + f_c^\downarrow = 3$ ($f_c^\uparrow = 2, f_c^\downarrow = 1$). The magnetic field is (a)-(d) $B = 2$ T; (e) $B = 1.96$ T; (f) $B = 1.25$ T.

proximation. The spin-resolved Landau levels in the QPC constriction depopulate one by one leading to the AB oscillations with the same periodicity as the one calculated without the exchange-correlation term. The corresponding wave function distributions for spin resolved electrons for $f_c = f_c^\uparrow + f_c^\downarrow = 3$ ($f_c^\uparrow = 2, f_c^\downarrow = 1$) are shown in Fig. 6. They also show the same features as those for spinless interacting electrons in the Hartree approximation, namely, adiabatic character of transport for the lowest f_c states, little intermode scattering as well as an absence of the compressible island in the center of the interferometer.

The conductance of the AB interferometer as a func-

tion of voltage applied to the gate defining the dot, V_g , is shown in Fig. 7 for spinless electrons for $f_c = 1, 2$, as well as for the spin-resolved case $f_c = 3$ ($f_c^\uparrow = 2, f_c^\downarrow = 1$). The DOS of interacting electrons, as in the case when magnetic field was varied, shows pinning of the weakly coupled narrow resonant states (situated inside the dot) to the Fermi level. Also, as in the case when B was varied, the conductance of noninteracting and interacting electrons (both spin-degenerate and spin-resolved) is practically the same. Every time a broad resonant level crosses E_F , the conductance exhibits maximum (see Fig. 7 (b), (c)). The ratio of the periods of the oscillations for both $f_c = 1$ and $f_c = 2$ is fully consistent with the conventional AB formula (2), $\Delta V_g^1 / \Delta V_g^2 = B^2 / B^1$ (note that the dot area varies approximately linearly with variation of the gate voltage of the side gate, $\Delta S = \alpha \Delta V_g^{17}$; indexes 1,2 correspond to $f_c = 1, 2$). Finally we notice that even though each AB resonance is mediated by a single level, the number of electrons in the dot between two consecutive peaks decreases by more than one, see Fig. 7 (a). These electrons are those that depopulate the states inside the dot (narrow resonances in the DOS, Fig. 2 (c)) and thus are not manifest in the conductance.

IV. DISCUSSION.

The results of the conductance calculations based on the Hartree and spin-DFT approaches presented in the previous section for $f_c \geq 1$ are in excellent agreement with the conventional AB formula, Eq. (1) predicting the same periodicity regardless of the number of the fully transmitted channels f_c . This is in obvious disagreement with the experiments^{2,3} that show a deviation from the conventional AB periodicity by a factor of $1/f_c$, Eq. (3). Besides, the AB calculated periodicity as a function of the gate voltage V_g is consistent with the conventional AB formula (2), which also contradicts to the experimental findings showing the same periodicity for all f_c independent of the magnetic field. In our discussion of the validity of the present approach, we argued that, as far as the conductance is concerned, the present method is justified for the case of the strong coupling when the conductance of the device exceeds the conductance unit, $G > G_0$, such that the electron number inside the structure is not expected to be quantized. However, our calculations for $f_c \geq 1$ do not recover the experimental conductance even though the total conductance of the system exceeds G_0 . What is the reason for this discrepancy?

We argue that inability of the “standard approach” to recover the experimental periodicity is an indirect evidence that, even though $G > G_0$, the electron charge in the interferometer is quantized and thus the Coulomb blockade effects become dominant in the conductance. This is because of the adiabatic character of the transport when the lowest f_c states pass through the interferometer with the transmission coefficient close to one, see Figs. 4,5,6. The highest state passing through the

QPCs, $f_c + 1$, (giving rise to the AB oscillations in the transition regions between the plateaus) becomes thus effectively decoupled from the remaining f_c states that pass through the interferometer practically without reflection. Therefore the AB interferometer effectively confines only electrons belonging to the highest ($f_c + 1$) subband passing through QPC. Because the conductance of this state is always smaller than one, the dot is in the weak coupling regime, even though the total dot conductance is larger than G_0 (due to the lower f_c states that pass adiabatically through the interferometer). As a result, the electron charge inside the dot becomes quantized and transport through the interferometer becomes strongly affected by the Coulomb blockade effect.

Note that manifestation of the Coulomb blockade effects in the conductance of open dots is not limited to the edge state regime only. Liang *et al.*¹⁵ demonstrated that the adiabatic transport regime can be achieved in an open quantum dot even at zero field leading to the dot conductance being dominated by combined charging and ballistic transport within a wide range $0 < G < 6e^2/h$. The dot of Ref. 15 was designed such that the intermode scattering was practically absent. As a result, the lowest f_c states propagated through the dot adiabatically with very little reflection, whereas highest states with the transmission $T < 1$ gave rise to the Coulomb blockade effects in the conductance.

We argued in Sec. II that while the present “standard approach” is not expected to describe single-electron tunneling effects (leading to the Coulomb blockade peaks in the conductance), one can expect that it correctly reproduces a global electrostatics of the interferometer and microscopic structure of the quantum mechanical edge states regardless whether the conductance is dominated by a single-electron charging or not. In its turn, such information can be a basis for phenomenological models aiming at description of the effects of single-electron charging in the AB interferometer.

Such model calculations have been recently reported by Rosenow and Halperin who studied the effect of the single electron charging on the periodicity of the AB interferometer⁴. In the absence of detailed microscopic picture of the edge state structure in the interferometer, the authors considered several possible scenarios of coupling between the edge states in the leads and states in the island. The important feature of their model was the presence of the compressible region in the center of the island. Our macroscopic calculations however do not support the assumption of the formation of the compressible strip inside the interferometer. Our calculations for $f_c \geq 1$ demonstrate only the onset of the formation of the compressible region where just a few resonant levels of the dot become pinned to the Fermi energy. The formation of the compressible region inside the interferometer occurs at larger fields corresponding to $f_c = 0$ (where however the conductance is dominated by the single-electron effects anyway because $G < G_0$). Note that Dharma-wardana *et al.*'s model¹³ of single electron

charging in the open AB interferometer does not seem to rely on the presence of the compressible island inside the dot.

A microscopic picture emerging from our calculation can be summarized as follows.

(i) The lowest f_c states pass through the QPC almost adiabatically contributing very little to the conductance oscillations (see Fig. 4 (d) and Fig. 6 (a)-(c)).

(ii) The state $f_c + 1$ passes through the interferometer with the transmission probability $0 < T < 1$ giving rise to the transition region between the conductance plateaus that is modulated by the AB oscillations. Inside the interferometer this state retains its edge-state character (see Fig. 4 (e) and Fig. 6 (d)). The AB oscillations are related to excitation of the resonant states of the dot that are situated close to the dot boundary and thus are strongly coupled to the leads. These states are manifest in the density of states as relatively broad peaks with broadening $\Gamma \sim kT$ (see Figs. 2,3,7).

(iii) The $f_c + 1$ state (and, to a lesser extent, all lowest f_c states) also excite very narrow resonant states with broadening $\Gamma \ll kT$ situated inside the island and thus weakly coupled to the leads (see Figs. 2,3,7). These states are pinned to the Fermi energy and the excitation of these states corresponds to the onset of formation of the compressible island inside the interferometer. Note however that compressible island inside the interferometer forms at much larger fields, see inset to Fig. 1 (d). Because both broad and narrow states correspond to the addition (or subtraction) of one electron to (or from) the dot, both of them can contribute to single-electron charging giving rise to modification of the conventional AB periodicity according to Eq. (3).

(iv) Finally, the $f_c + 2$ state is almost completely reflected by the QPC, see (see Fig. 4 (f) and Fig. 6 (e)). This state might or might not form a compressible strip in the leads (depending on whether it is respectively the last filled LL or not). However, because of the weak coupling to the states in the dot, the compressibility of this state has a little significance for the transport through the interferometer.

Finally we stress that our approach corresponds to the coherent electron transport through the interferometer. It does not account for incoherent processes such as spin flips and interlevel scattering that might lead to redistribution of electrons between outer (broad) and inner (narrow) resonant states in the dot. Such electron transfer between different LLs is shown to influence an addition spectrum of a closed (strongly Coulomb-blockaded) dot²⁷. However, in the case of open dot considered in this study it is not clear whether such processes would significantly affect the conductance of the interferometer, because the dwell time of the electrons in the open dot might be much smaller than inelastic scattering time associated with the interlevel relaxation.

V. CONCLUSION.

We provide a microscopic picture of the quantum transport in the Aharonov-Bohm interferometer taking into account electron interaction within the Hartree and the spin-DFT approximations. We discuss the structure of the edge states for different numbers of the Landau levels in the leads, structure of the states in the dot, coupling between the states in the dot and the leads, and the formation of compressible/incompressible strips in the interferometer. We discuss the applicability of our approach and argue that it provides a reliable description of a global electrostatics of the interferometer and a microscopic structure of the quantum mechanical edge states and coupling between them. On the other hand, the present approach is not expected to reproduce the conductance in the weak coupling regime of the Coulomb blockade, if the electron number inside the interferometer becomes quantized. We compare our conductance calculation with the experiment^{2,3} and argue that the inability of the present approach to reproduce the unexpected periodicity of the AB oscillations, Eq. (3), can be taken as an indirect evidence that this periodicity is caused by the Coulomb blockade-type effects.

Our transport calculations thus demonstrate that an accurate description of the conductance of the AB in-

terferometer would require theories that go beyond the “standard approach”²⁴ based on the ground-state DFT in the Landauer formula that was utilized in the present paper. Such the theories (as e.g. reported in Refs. 4,13) essentially rely on specific phenomenological models of the states in the leads and in the central island and their coupling in the interferometer. Our work, therefore, provides a basis for such the theories, giving a detailed microscopic description of the propagating states and the global electrostatics in the system at hand. Such a microscopic description is summarized in Sec. IV. In particular, our findings does not directly support the model of Rosenow and Halperin that relies on the existence of the compressible island inside the interferometer and its coupling to the leads. Our findings thus indicate that an accurate explanation of the unexpected periodicity of the AB oscillations might need exploring alternative theories based on the microscopic picture of interesting electrons developed in the present paper.

Acknowledgement. We are thankful V. Goldman for drawing our attention to the current problem. We appreciate valuable discussions with V. Goldman, T. Heinzl, A. Sachrajda. We acknowledge access to computational facilities of the National Supercomputer Center (Linköping) provided through SNIC.

-
- ¹ F. E. Camino, W. Zhou, and V. J. Goldman, Phys. Rev. Lett. **95**, 246802 (2005); F. E. Camino, W. Zhou, and V. J. Goldman, Phys. Rev. B **72**, 075342 (2005).
- ² F. E. Camino, Wei Zhou, and V. J. Goldman, Phys. Rev. B **72**, 155313 (2005).
- ³ F. E. Camino, Wei Zhou, and V. J. Goldman, Phys. Rev. B **76**, 155305 (2007).
- ⁴ B. Rosenow and B. I. Halperin, Phys. Rev. Lett. **98**, 106801 (2007).
- ⁵ S. Das Sarma, M. Freedman, and Ch. Nayak, Phys. Rev. Lett. **94**, 166802 (2005).
- ⁶ J. B. Miller, I. P. Radu, D. M. Zumbühl, E. M. Levenson-Falk, M. A. Kastner, Ch. M. Marcus, L. N. Pfeiffer, and K. W. West, Nature Physics **3**, 561 (2007).
- ⁷ S. Das Sarma, M. Freedman, Ch. Nayak, S. H. Simon, A. Stern, Rev. Mod. Phys., to be published (arXiv:0707.1889v1 [cond-mat.str-el]).
- ⁸ B. J. van Wees, L. P. Kouwenhoven, C. J. P. M. Harmans, J. G. Williamson, C. E. Timmering, M. E. I. Broekaart, C. T. Foxon, and J. J. Harris, Phys. Rev. Lett. **62**, 2523 (1989).
- ⁹ B. W. Alphenaar, A. A. M. Staring, H. van Houten, M. A. A. Mabeoone, O. J. A. Buyk, and C.T. Foxon, Phys. Rev. B **46**, 7236(R) (1992).
- ¹⁰ R. P. Taylor, A. S. Sachrajda, P. Zawadzki, P. T. Coleridge, and J. A. Adams, Phys. Rev. Lett. **69**, 1989 (1992).
- ¹¹ M. Field, C. G. Smith, M. Pepper, D. A. Ritchie, J. E. F. Frost, G. A. C. Jones and D. G. Hasko, J. Phys.: Condens. Matter **6** L273 (1994).
- ¹² J. Davies, *The Physics of Low-Dimensional Semiconductors*, (Cambridge University Press, Cambridge, 1998).
- ¹³ M. W. C. Dharma-wardana, R. P. Taylor and A. S. Sachrajda, Solid State Comm. **84**, 631 (1992).
- ¹⁴ M. Kataoka, C. J. B. Ford, G. Faini, D. Mailly, M. Y. Simmons and D. A. Ritchie, Phys. Rev. B **62**, 4817 (R) (2000); M. Kataoka, C. J. B. Ford, G. Faini, D. Mailly, M. Y. Simmons, D. R. Mace, C. -T. Liang and D. A. Ritchie, Phys. Rev. Lett. **83**, 160 (1999); C. J. B. Ford, P. J. Simpson, I. Zailer, D. R. Mace, M. Yosefin, M. Pepper, D. A. Ritchie, J. E. F. Frost, M. P. Grimshaw and G. A. C. Jones, Phys. Rev. B **49**, 17456 (1994).
- ¹⁵ C.-T. Liang, M. Y. Simmons, C. G. Smith, G.-H. Kim, D. A. Ritchie and M. Pepper, Phys. Rev. Lett. **81** 3507 (1998); O. A. Tkachenko, V. A. Tkachenko, D. G. Baksheyev, C.-T. Liang, M. Y. Simmons, C. G. Smith, D. A. Ritchie, Gil-Ho Kim, and M. Pepper, J. Phys.: Condens. Matter **13**, 9515 (2001).
- ¹⁶ V. J. Goldman, J. Liu and A. Zaslavsky, Phys. Rev. B **77**, 115328 (2008).
- ¹⁷ S. Ihnatsenka, I. V. Zozoulenko and M. Willander, Phys. Rev. B **75**, 235307 (2007).
- ¹⁸ S. Ihnatsenka and I. V. Zozoulenko, Phys. Rev. B **76**, 045338 (2007).
- ¹⁹ S. Ihnatsenka and I. V. Zozoulenko, unpublished (arXiv:0801.1820v1 [cond-mat.mes-hall]).
- ²⁰ S. Ihnatsenka and I. V. Zozoulenko, Phys. Rev. Lett. **99**, 166801 (2007).
- ²¹ G. F. Giuliani and G. Vignale, *Quantum Theory of the Electron Liquid*, (Cambridge University Press, Cambridge, 2005).
- ²² B. Tanatar and D. M. Ceperley, Phys. Rev. B **39**, 5005, (1989).

- ²³ S. Ihnatsenka and I. V. Zozoulenko, Phys. Rev. B **73**, 075331 (2006); S. Ihnatsenka and I. V. Zozoulenko, Phys. Rev. B **73** 155314 (2006).
- ²⁴ M. Koentopp, C. Chang, K. Burke and R. Car, J. Phys.: Condens. Matter **20**, 083203 (2008).
- ²⁵ F. Evers, F. Weigend, and M. Koentopp, Phys. Rev. B **69**, 235411 (2004); C. Toher, A. Filippetti, S. Sanvito, and K. Burke, Phys. Rev. Lett. **95**, 146402 (2005); M. Koentopp, K. Burke, F. Evers, Phys. Rev. B **73**, 121403(R) (2006); J. J. Palacios, Phys. Rev. B **72**, 125424 (2005).
- ²⁶ I. Karakurt, V. J. Goldman, J. Liu, and A. Zaslavsky, Phys. Rev. Lett. **87**, 146801 (2001); M. Kataoka and C. J. B. Ford, Phys. Rev. Lett. **92**, 199703 (2004); V. J. Goldman, Phys. Rev. Lett. **92**, 199704 (2004); S. Ihnatsenka and I. V. Zozoulenko, Phys. Rev. B **74**, 201303(R) (2006).
- ²⁷ P. L. McEuen, E. B. Foxman, J. Kinaret, U. Meirav, M. A. Kastner, N. S. Wingreen, and S. J. Wind, Phys. Rev. B **45**, 11419(R) (1992).